Microstructure of single-phase cobalt and manganese oxide spinel $Mn_{3-x}Co_xO_4$ ceramics

N. El Horr *, S. Guillemet-Fritsch, A. Rousset, H. Bordeneuve, C. Tenailleau

Institut Carnot CIRIMAT, Université Paul Sabatier, UMR CNRS 5085, 118 route de Narbonne, 31062 Toulouse Cedex 9, France

Abstract

This paper reports microstructural studies of single-phase $Mn_{3-x}Co_xO_4$ ($0.98 \leq x \leq 2.93$) spinel ceramics using transmission electron microscopy (TEM) and energy dispersive X-ray spectroscopy (EDX). These ceramics were obtained by conventional sintering or by spark plasma sintering (SPS) of powders prepared by thermal decomposition of coprecipitated oxalate precursors. For $x < 1.78$ or $x \geq 1.78$, the monophasic ceramics correspond respectively to quadratic (Q) or cubic (C) spinel structure. The ferroelastic character of the structural phase transition from C to Q is highlighted by specific microstructural features. The effect of chemical composition and heat treatment conditions on the microstructure and essentially on the presence and the characteristics of twins were investigated. The coherent twin interfaces are parallel to (1 1 2) planes in the Q cell. Twins can correspond to: tweeds, single lamellae (widths: 5–306 nm) arranged parallel to each other, large lamellae (widths: 69–928 nm) internally twinned and sometimes arranged in cyclic forms (triangular shapes).

Keywords: Cobalt manganite; Sintering; Microstructure; Twins; Electron microscopy

1. Introduction

Manganites have been of great interest to materials researchers since the 1950s.[1–4] Indeed, in addition to their wide range of chemical compositions and their broad variety of structural phases (with a high number of possible cation distributions), they can also exhibit a large range of physical, chemical, electric, magnetic properties, etc.

Mixed-valence transition-metal manganites with a spinel structure $Mn_{3-x}Me_xO_4$ (Me = Co, Ni, Fe, Cu, Zn, Cr and Zr) are known as basic materials used to manufacture thermistors with Negative Temperature Coefficient (NTC).[5–9] This specificity makes them highly attractive for several technology domains (microelectronics, optoelectronics, etc.) and they are thus used in many industrial applications[10–17]: temperature sensors, time delay elements, infrared detectors, voltage regulators, etc.

Apart from the numerous applications arising from spinel manganites, it is important to note that these materials are also attracting considerable interest in fundamental research due to the complexity of the relationships that exist between, firstly, the chemical methods used to prepare powders and ceramics, secondly, the structures (and in particular cation distribution), microstructures (density, grain size, grain morphology, presence of several phases, presence of defects: precipitates, twins, etc.) of the obtained products and thirdly, their many physical and chemical properties: electric, magnetic, etc. Judicious control of these relationships could provide new ways to obtain spinel manganites with controlled properties.

The microstructure of spinel manganite ceramics has been the subject of many studies,[7–9,18–33] many of which were performed in our laboratory. In most cases, these manganites are obtained by sintering powders prepared either by hydrothermal methods (thermal decomposition of precursors produced by coprecipitation) or by traditional methods and correspond to binary systems: Mn–Ni–O, Mn–Fe–O, Mn–Zn–O, etc. to ternary systems: Mn–Ni–Co–O, Mn–Ni–Cu–O, Mn–Ni–Zn–O, Mn–Ni–Zr–O, Mn–Ni–Fe–O, Mn–Ni–In–O, etc. and systems with four or more cations: Mn–Ni–Co–Al–O, Mn–Ni–Co–Zn–O, Mn–Ni–Fe–Cr–O, Mn–Ni–Co–Cu–Si–O, etc.

Amongst these studies, we note that the presence of defects such as precipitates or twins, in these manganites, and also the

* Corresponding author. Tel.: +33 5 62 25 82 53; fax: +33 5 62 25 82 77.
E-mail address: nahida.el-horr@iut-tlse3.fr (N. El Horr).

http://dx.doi.org/10.1016/j.jeurceramsoc.2013.08.010

characteristics of the observed twins, depend on the chemical composition of the samples and their heat treatment conditions. Additionally, in some cases, these defects can play an important role in controlling the electrical properties of manganites.

Very few studies[34–41] had been performed on the Mn–Co–O system before the works conducted in our laboratory. They have involved more detailed works on films and powders than on ceramics. The recent works on $Mn_{3-x}Co_xO_4$ ceramics done in our laboratory and which were the subject of several publications, have focused on structures (identification of phases and cation distributions), along with magnetic and electrical properties.[42–46] We note that the electrical properties studies[42,46] of single-phase $Mn_{3-x}Co_xO_4$ spinel ceramics, obtained by conventional sintering or by SPS, had shown that these ceramics are semiconductors and possess interesting electrical characteristics making them attractive materials for industrial applications as NTC thermistors. Also, these studies showed that for measurements made at 25 °C, the minimum resistivity ($\rho_{25°C}$) value is of about 387 Ω.cm for $x = 1.78$ and this $\rho_{25°C}$ value increases in a much more intense manner on the zone where $x < 1.78$ (particularly for $0.98 \geq x > 1.54$) then on the zone where $x > 1.78$ (for $x = 0.98$, $\rho_{25°C} = 49{,}552\ \Omega$ cm and for $x = 2.93$, $\rho_{25°C} = 5020\ \Omega$ cm). Electrical conduction could take place by the polarons hopping between cations.

To our knowledge, the work reported in this article corresponds to the first microstructural study of cobalt manganese oxide ceramics, $Mn_{3-x}Co_xO_4$.

2. Experimental

2.1. Sample preparation

As has been described in detail by H. Bordeneuve et al.[42], oxalic precursors, $Mn_{1-\alpha}Co_\alpha C_2O_4{\cdot}nH_2O$, were first obtained by the coprecipitation of an aqueous solution of ammonium oxalate and a mixture of manganese and cobalt nitrates in proportions varying according to the chemical composition of the final product. Thus, the resulting solution was aged for 30 min, then filtered, washed with water and dried in air at 90 °C. Oxide powders were produced by thermal decomposition of coprecipitated oxalate precursors (in air at 800 °C). Pellets of 6 mm in diameter were obtained by pressing oxide powders at 500 MPa. After that, two types of sintering were used: conventional sintering and Spark Plasma Sintering (SPS). As has been previously reported in detail,[42,47] producing single-phase cobalt manganese oxide ceramics is difficult to achieve and requires an adaptation of the sintering conditions according to the desired chemical composition of the sample.

For $x < 1.78$ and taking into account the phase diagram of the Mn_3O_4–Co_3O_4 system (reported in previous works[42,48]), single-phase ceramic preparation is restricted by the many structural transformations taking place at various temperatures. Thus, as has been previously described,[42,47] the sintering process must be carried out at high temperature (between 1160 °C and 1280 °C in air, for the samples which are the object of this study) in order to be placed in the zone of the single cubic (C) spinel phase and to give the ceramic sufficient densification. Additionally, the samples must be quenched to avoid obtaining two-phase samples. In fact, when they have been cooled at different rates (i.e. the samples have not been quenched), the obtained ceramics were biphasic. The temperature of quenching could be a little lower than the sintering temperature (but still in the domain of the single C phase) to avoid cracking the samples. So, for $x < 1.78$, quadratic (Q) single-phase ceramics were successfully produced under the sintering conditions reported in Table 2.

For samples corresponding to $x = 1.54$ and for which the C spinel phase exists at lower temperatures than for $x < 1.54$ (as has been described previously),[42,47] the SPS method has also been used (Table 2) in addition to conventional sintering.

For $x \geq 1.78$, the preparation of single-phase ceramics is restricted by the fact that the reduction of the C spinel phase occurs at lower temperatures than in the domain that corresponds to $x < 1.78$, making it difficult to obtain single-phase ceramics with high densities by conventional sintering.[42,47] So, in this case, there are two possibilities to conduct the sintering of the samples:

- conventional sintering with a sintering temperature higher than the sample reduction temperature but with a cooling rate low enough to reoxidize the sample.
- SPS sintering which allowing us to decrease the optimum sintering temperature compared to the conventional method.

These two possibilities have proven to be valid for $x = 1.78$, but, as the x value increases, the reoxidation of the samples becomes more difficult with the conventional method. So, for $x > 1.78$, only the SPS sintering has led to us, obtaining C single-phase ceramics with high densities.[42,47] All sintering conditions are reported in Table 2.

For SPS sintering, the apparatus used was a Sumitomo 2080 (PNF2 CNRS platform available at the University of Toulouse, France). The oxide powders were pre-compacted, then placed in a graphite die and heated under vacuum at temperatures between 700 and 750 °C, depending on sample composition and under a pressure of 50 MPa. The pressure was maintained constant until the end of the dwell time at 700 or 750 °C. After that, the pressure was removed, and the sample was cooled to room temperature by shutting down the power supply. The resulting samples were polished to remove the (Co,Mn)O thin layer deposited on surface samples during sintering (as has been described previously).[42,47]

The densification values[46] of obtained samples were between 93% and 94% for samples subject to conventional sintering, and between 95% and 97% for those sintered by SPS (Table 1).

2.2. Sample characterization

A Brucker D4 powder diffractometer was used to determine sample X-ray diffraction (XRD) patterns. The diffractometer operated with an emitting source of Cu ($K\alpha_1$,α_2 mean = 1.5418 Å).

We noted that the ceramic samples sintered by SPS, along with those sintered by conventional method, but with low cobalt contents, belong to brittle materials (like glass) and hence, the preparation of these samples for transmission electron

Table 1
Sintering conditions, space group and cell parameters determined by XRD[42,47] of $Mn_{3-x}Co_xO_4$ ceramics. The relative density[46] (d_R), average grain size (D_{av}) and cell deformation (cell def) are also reported.

x	Sintering method	d_R (%)	Phase	D_{av} (μm)	a' (nm)	c (nm)	c/a'	Cell def[e] (%)
0.98	conv[a]	94	Q[c]	22	0.80956 (3)	0.92052 (4)	1.13706 (9)	13.7
1.27	conv	93	Q	13.5	0.81163 (5)	0.89743 (7)	1.1057 (2)	10.6
1.54	conv	93	Q	17.3	0.82258 (3)	0.85998 (4)	1.04547 (9)	4.6
1.54	SPS[b]	95	Q	1.00	0.82250 (2)	0.86020 (4)	1.04584 (7)	4.6
1.66	conv	94	Q	12.0	0.82481 (4)	0.85081 (4)	1.03152 (9)	3.2
1.78	conv	94	C[d]	10.0	0.83183 (4)		1	
1.78	SPS	95	C	0.67	0.83130 (1)		1	
1.99	SPS	95	C	0.56	0.82760 (9)		1	
2.22	SPS	97	C	0.44	0.82211 (3)		1	
2.93	SPS	96	C	0.34	0.80995 (7)		1	

[a] conv: conventional method.
[b] SPS: Spark plasma sintering.
[c] Q: quadratic with the space group $I4_1/amd$.
[d] C: cubic with the space group Fd-3m.
[e] Cell def (%) = $(c/a' - 1) \times 100$.

microscopy (TEM) observations requires a lot of ability and resourcefulness. The method used for TEM sample preparation is as follows: a diamond saw (ESCIL 3032-4) was used to obtain a sample block from each pellet, which was then placed inside a brass tube (of fine diameter ~3 mm) and bound with an epoxy resin (Gatan G1). The resin was polymerized at 50 °C overnight, then 500 μm thick discs were collected by slicing the tube using the same diamond saw. To make each sample electron-transparent, i.e., to reduce its thickness to approximately 100 nm, each sample was mechanically polished (using ESCIL: ESC 300 GTL), then concave dimple polished (with a EA-Fishione – model 2000 – polishing liquid: solution with diamond in suspension) and finally ion beam-thinned (using GATAN PIPS).

The ceramic samples were observed using a JEOL JEM 2010 electron microscope (200 kV – emitter: single crystal LaB6 tip – maximum resolution: 0.23 nm point–point and 0.14 nm line–line). The chemical composition of each sample was analyzed both qualitatively and quantitatively (simultaneously with TEM observations) by using a Tracor Voyager Energy Dispersive X-ray analyzer (EDX). Probe size may be reduced to 7 nm.

For each sample, granulometric analyses and twin lamellar thickness of TEM images were performed using imageJ software.[49]

3. Results

As is reported in Table 1, all obtained samples correspond to C spinel structure (Fd-3m space group) for $x \geq 1.78$ and to Q spinel structure ($I4_1/amd$ space group) for $x < 1.78$. To facilitate the comparison between Q and C spinel cells, the Q cell was converted to a bigger unit cell with $a' = a\sqrt{2}$ and $c' = c$ and the c/a' deformation was evaluated for each sample.

3.1. Grain sizes (GSs)

Before describing the GS of ceramic samples, we recall that the GS of initial powders,[47] for which $0.98 \leq x \leq 2.93$, present a relatively wide GS distribution and vary as follows: GSs are of the order of a few hundred nm for $x = 0.98$. They then increase with increasing x from 0.98 to 1.27, where they reach a maximum (without exceeding a maximum GS value of about 600 nm). They then decrease as x varies from 1.27 to 2.72, thus reaching values close to a few tens of nm. From this latter value of x, GS values once more increase up to $x = 2.93$ and become of the order of a few hundred nm.

3.1.1. Samples with conventional sintering ($0.98 \leq x \leq 1.78$)

TEM observations of the ceramic samples reveal that the grains possess polyhedral shapes and are mostly equiaxed. Each sample presents a wide dispersion of GSs. Minimum GS is about few microns (1– 4 μm) for all samples but maximum GS is respectively 40 μm, 25 μm, 33 μm and 19 μm for $x = 0.98$, $x = 1.27$, 1.54 and 1.78, according to the sintering conditions and the GS of the initial powders. The average GSs (D_{av}) of these ceramic samples are reported in Table 1.

3.1.2. Samples with SPS sintering ($1.54 \leq x \leq 2.93$)

These samples also contain grains with polyhedral shapes and which are mostly equiaxed. GSs are polydispersed and very small compared to those of samples obtained by conventional sintering. They vary between 300 nm and 1.7 μm for $x = 1.54$ and decrease systematically with increasing x value, i.e., with increasing Co content. Thus, the minimum and maximum GS values are respectively 135–1210 nm, 103–1016 nm, 95–781 nm, and 76–611 nm for $x = 1.78$, $x = 1.99$, $x = 2.22$ and $x = 2.93$. The GS variation of the final samples is due to changes in sintering conditions and also in the GSs of the initial powders. The D_{av} values of these ceramics are reported in Table 1.

3.2. Defects

Samples with $x < 1.78$ show grains with high densities of two-dimensional structural defects. Depending on the concerned sample, these latter correspond to some of the following types of defects:

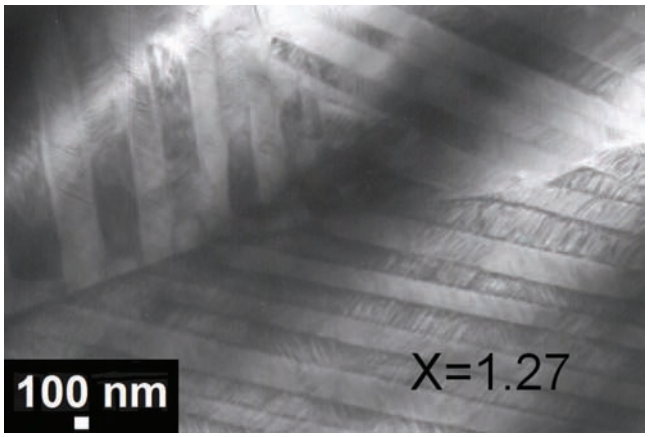

Fig. 1. Bright field TEM image of a single quadratic phase $Mn_{3-x}Co_xO_4$ ceramic sample for $x = 1.27$ showing a triple junction and the intense presence in each grain of large lamellae (L_{IT}) which are internally twinned (i.e. containing fine lamellae (l)).

- twins, in the form of lamellae (L) parallel to each other (each lamella corresponds to a single atomic domain).
- large lamellae (L_{IT}) which are internally twinned (i.e., containing fine lamellae (l)).
- tweeds (very fine lamellae arranged in two mutually perpendicular directions).

3.2.1. Monophasic samples with Q structure

A single Q phase was obtained for samples with $x < 1.78$ that were sintered by the conventional method or by SPS sintering. The lattice parameters and the c/a' deformation of these samples are reported in Table 1. Quantitative chemical analysis by EDX had shown that each of these samples is homogeneous. The experimental values of x are reported in Table 2. They fit well with the expected values of x corresponding to theoretical chemical compositions.

- samples with $0.98 \leq x < 1.54$: These samples contain almost L_{IT} lamellae (Figs. 1 and 2) and are sometimes arranged in cyclic forms corresponding to triangles (Fig. 3). To our knowledge, this triangle arrangement shape of L_{IT}, corresponds to a type of arrangement observed for the first time in manganites. This arrangement could be explained by the existence of a 3-fold symmetry axis in the C phase (high-temperature phase) with space group Fd-3m. The widths of L_{IT} and also the widths of the l fine lamellae (inside L_{IT}) are reported in Table 2. The maximum value of L_{IT} width is greatly decreased with increasing x value from 0.98 to 1.27.
- sample with $x = 1.54$ sintered by conventional method: This sample contains only approximately L lamellae (Fig. 4). The forms of these lamellae correspond to either right-angled twins (i.e., domains with practically right-angled twin walls) or needle-shaped twins (i.e., the trajectories of the twin walls are like needles) (Fig. 5). This is quite typical for a ferroelastic transition.[50–53] The widths of these lamellae are reported in Table 2.
- sample with $x = 1.54$ sintered by SPS: This sample contains only L lamellae (Fig. 6). The lamella widths are reported in Table 2 and are much finer than those of the sample sintered by the conventional method. The lattice parameters and the c/a' deformation are almost the same as those obtained with conventional sintering for $x = 1.54$. Also, the type of structural defects does not change and corresponds to L lamellae. But the SPS sintering generated a significant decrease in GS compared to conventional sintering, which could be the cause of the drop in lamella widths, as was reported in the literature concerning the effect of GS on the widths of twin lamellae.[54–57]

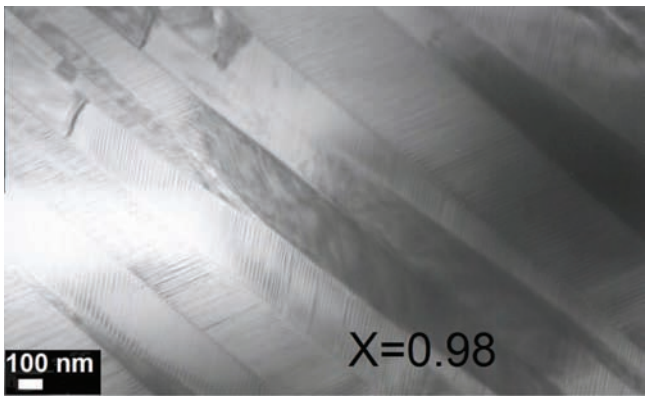

Fig. 2. Bright field TEM image of a single quadratic phase $Mn_{3-x}Co_xO_4$ ceramic sample for $x = 0.98$ showing that the lamellae (L_{IT}) are much larger than those of ceramic sample with $x = 1.27$.

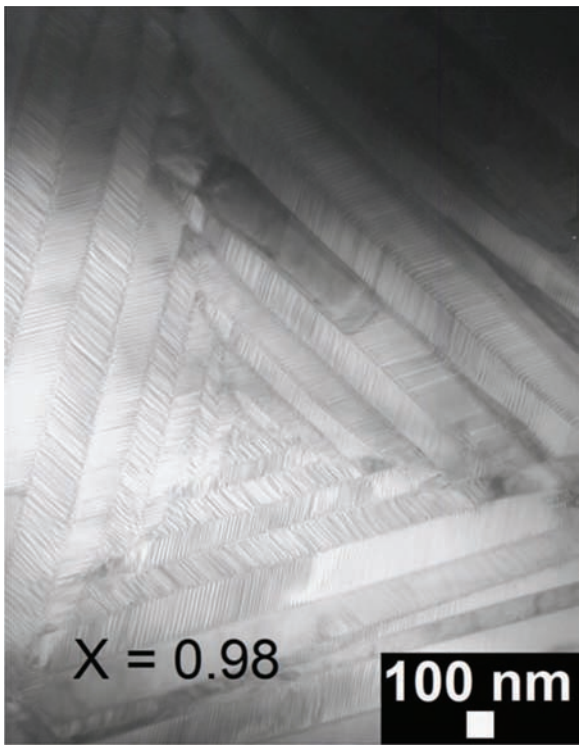

Fig. 3. Bright field TEM image of a single quadratic phase $Mn_{3-x}Co_xO_4$ ceramic sample for $x = 0.98$ showing L_{IT} lamellae arranged in a cyclic form corresponding to a triangle observed for the first time in manganites. This arrangement could be explained by the existence of a 3-fold symmetry axis in the C phase (high-temperature phase) with space group Fd-3m.

Table 2
Preparation conditions, structure and microstructural defects for monophasic ceramics. The theoretical (theor.) values of x (Co content in samples) and the experimental ones determined by energy dispersive X-ray analysis (EDX), are also reported.

x (theor. value)	Sintering method-sintering temperature (°C)	Cooling rate	Phase	Twin types	Lamella widths min–max (nm)	x value by EDX
0.98	conv[a]-1280	120 °C/h and air-quenched from T = 900 °C	Q[c]	L_{IT}[e]	77–928	0.95(3)
				l[f]	3–13	
1.27	conv-1180	120 °C/h and air-quenched from T = 800 °C	Q	L_{IT}	69–409	1.25(5)
				l	3–26	
1.54	conv-1180	air-quenched from T = 1180 °C	Q	L[g]	12–306	1.54(3)
1.54	SPS[b]-750	cut-off of the furnace	Q	L	5–45	1.55(3)
1.66	conv-1160	120 °C/h and air-quenched from T = 900 °C	Q	T[h]	2–14	1.64(3)
1.78	conv-1160	10 °C/h to 400 °C and 20 °C/h to 25 °C	C[d]	No defects		1.75(4)
1.78	SPS-750	Cut-off of the furnace	C	No defects		1.72(5)
1.99	SPS-750	Cut-off of the furnace	C	No defects		1.97(4)
2.22	SPS-700	Cut-off of the furnace	C	No defects		2.21(3)
2.93	SPS-700	Cut-off of the furnace	C	No defects		2.91(6)

[a] conv: conventional method.
[b] SPS: spark plasma sintering.
[c] Q: quadratic phase.
[d] C: cubic phase.
[e] L_{IT}: large lamellae which are internally twinning.
[f] l: the internal twins, i.e., twins which are inside each large lamella.
[g] L: lamellae without internal twins.
[h] T: tweed.

- sample with x = 1.66: This sample includes tweeds with high frequency (Fig. 7). These tweeds are very fine with widths varying from 2 to 14 nm.

Considering all samples, the domain walls (DW) of the internal twins (l) and also the DW of domains with no internal twins (L) belong to the type-I mechanical twin, meaning that the atomic arrangement of one domain is the mirror reflection of the other by the twin interface plane, corresponding to the (1 1 2) crystallographic plane for our samples. So, as had be shown in a previous study[21], and mentioned in other studies,[9,26] these DW (i.e., corresponding to L and l) constitute coherent twin boundaries. The DW of the L_{IT} large lamellae, however, form incoherent twin boundaries.

The type-I mechanical 1 1 2 twins are shown in the diffraction patterns reported in Fig. 8. The diagrams are indexed according to the Q cell, and correspond to the zone axes [1$\bar{1}$0] and [1$\bar{3}$1]. The presence of twins in sample microstructures is shown in these diagrams by a splitting of the reflections corresponding

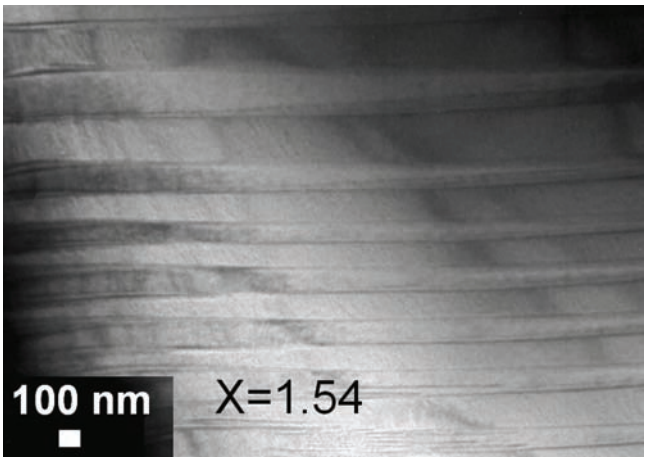

Fig. 4. Bright field TEM image of a single quadratic phase $Mn_{3-x}Co_xO_4$ ceramic sample for x = 1.54 (conventionally sintered) showing L lamellae (without internal twins) corresponding to right-angled twins (i.e., domains with practically right-angled twins walls). The maximum value of their widths is about a few hundred of nanometers.

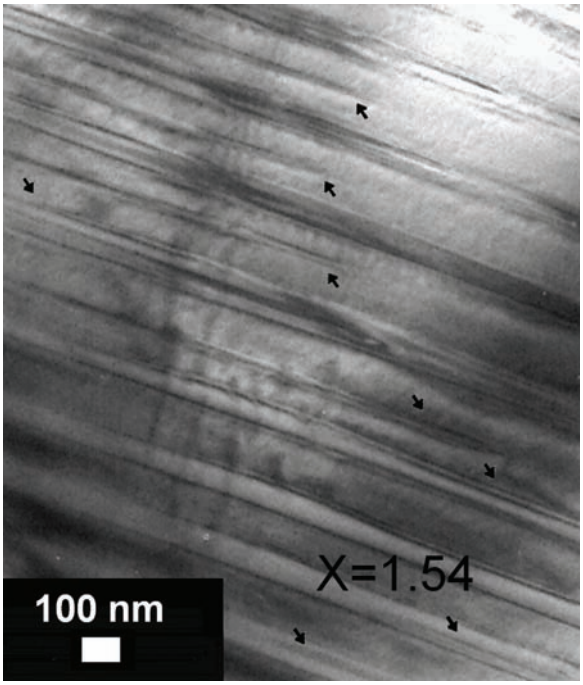

Fig. 5. Bright field TEM image of a single quadratic phase $Mn_{3-x}Co_xO_4$ ceramic sample for x = 1.54 (conventionally sintered) showing L lamellae corresponding to needle-shaped twins (i.e. the trajectories of the twin walls are like needles) and indicated by arrows.

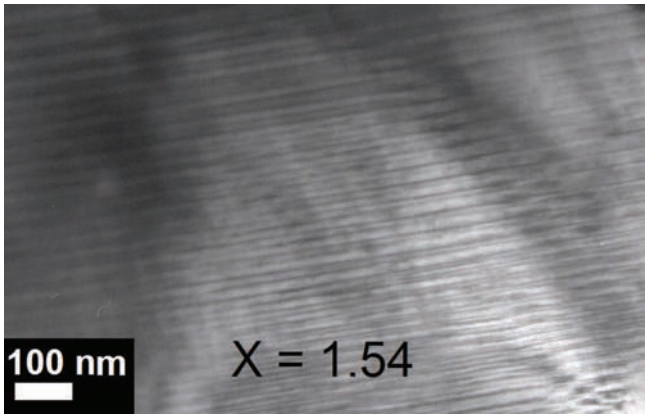

Fig. 6. Bright field TEM image of a single quadratic phase $Mn_{3-x}Co_xO_4$ ceramic sample for $x = 1.54$ (sintered by SPS) showing L lamellae that are very much finer (maximum width value is a few tens of nm) than those of the sample with the same value of x but conventionally sintered.

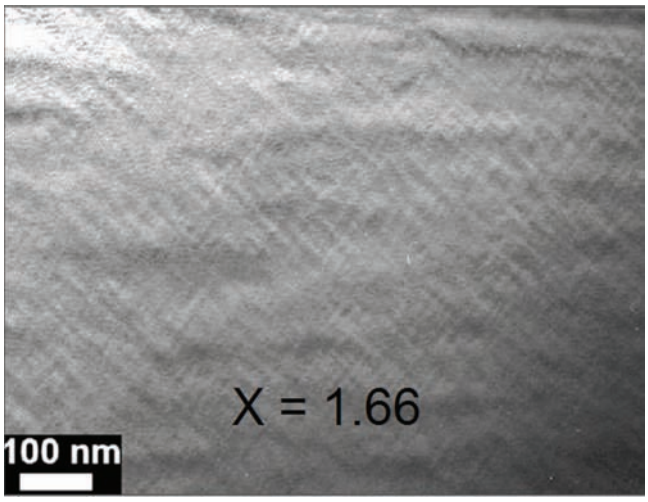

Fig. 7. Bright field TEM image of a single quadratic phase $Mn_{3-x}Co_xO_4$ ceramic sample for $x = 1.66$ showing the presence of defects corresponding to tweeds (very fine lamellae with widths of a few nm, and arranged in two mutually perpendicular directions).

to the diffraction of zones located on either side of the (1 1 2) twin interface plane (i.e., the twin boundary). Splitting magnitude increases with the distance from the center of the pattern. Non split reflections correspond to crystallographic rows perpendicular to the (1 1 2) twin interface plane.

3.2.2. Monophasic samples with C structure

A single C phase was obtained for samples with $x \geq 1.78$ and sintered by SPS sintering or by the conventional method (only for $x = 1.78$). The lattice parameters of these samples are reported in Table 1. Quantitative chemical analysis by EDX had shown that each of these samples is homogeneous. As shown in Table 2, for each sample, the experimental value of x fits well with that corresponding to the theoretical chemical compositions.

These samples (i.e., $x \geq 1.78$) differ from previous samples (i.e., $0.98 \leq x < 1.78$) in that they contain no defects (Figs. 9 and 10). We noted that, for $x = 1.78$, the two sintering methods (SPS and conventional sintering) lead to the production of samples free from defects (the only changes induced by the modification of the sintering method, correspond to a GS variation of the final samples, as mentioned above).

4. Discussion

Single-phase $Mn_{3-x}Co_xO_4$ ($0.98 \leq x \leq 2.93$) spinel ceramics present a variety of microstructural characteristics depending on the sample's chemical composition (i.e., value of x) and the type of heat treatment applied prior to obtaining the final product.

We recall that for $x < 1.78$ or $x \geq 1.78$, the monophasic ceramics correspond to Q ($I4_1/amd$ space group) or C (Fd-3m space group) spinel structures respectively. Q phase arises by the structural transition of C phase in agreement with the phase diagram of the Mn_3O_4–Co_3O_4 system.[42,48] This structural

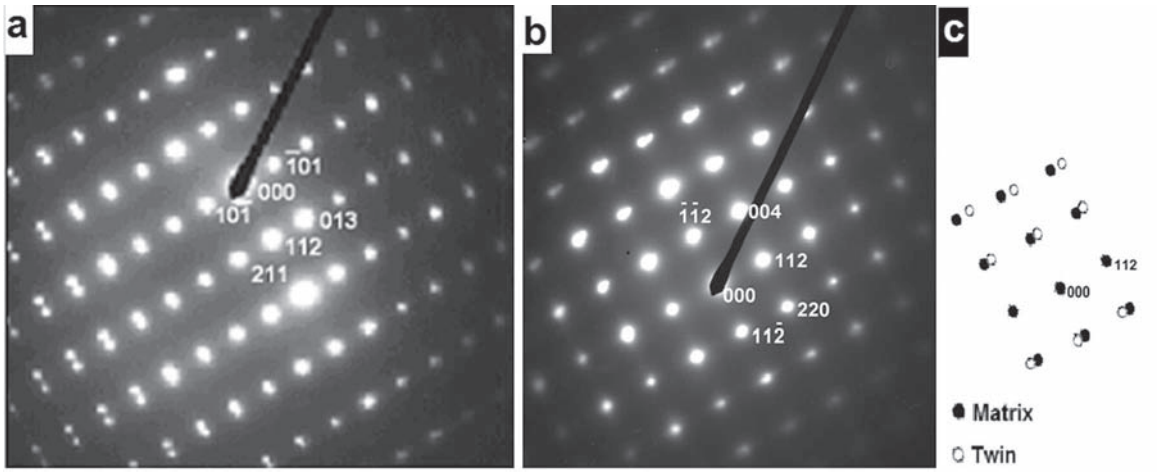

Fig. 8. Selected area electron diffraction (SAED) patterns of a single quadratic phase $Mn_{3-x}Co_xO_4$ ceramic sample for $x = 1.54$: (a) along the zone axis $[1\bar{3}1]$, (b) along the zone axis $[1\bar{1}0]$, and (c) shematic reproduction of a part of (b). These patterns exhibit splitting of spots (in such a way that there are spots corresponding to the matrix and other spots corresponding to twins which are deducted from the first ones by reflection from a plane mirror coinciding with the twin interface plane). The reflections that are not split correspond to crystallographic rows perpendicular to the (1 1 2) twin interface plane. The magnitude of splitting increases with the distance from the center of the pattern.

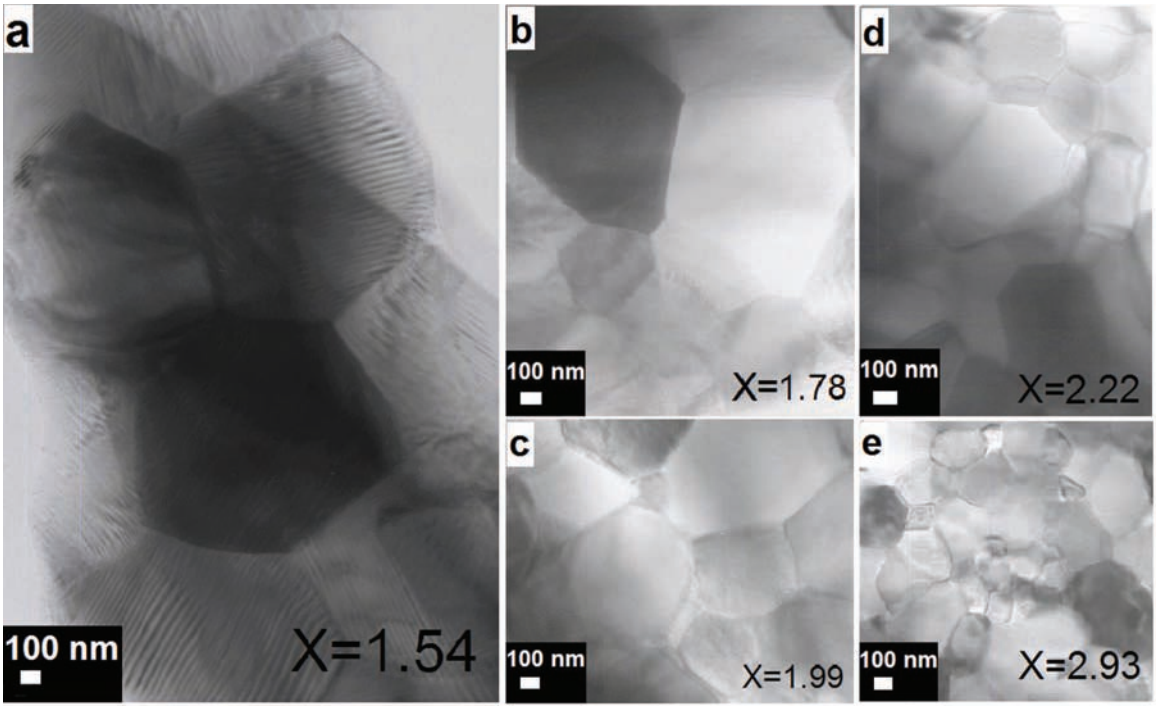

Fig. 9. Bright field TEM images of all samples sintered by SPS: (a) for $x = 1.54$, (b) for $x = 1.78$, (c) for $x = 1.99$, (d) for $x = 2.22$, and (e) for $x = 2.93$. They show that for $x \geq 1.78$, no twins defects were observed in the single cubic phase ceramic samples, unlike the case of the single quadratic phase ceramic sample with $x = 1.54$ and which contains twins lamellae, L.

phase transition is caused by the cooperative Jahn–Teller effect as in other manganite compounds.[21,22,26,58,59] The C structure is stable only at high temperatures and cannot be observed at room temperature after quenching in the manganese-rich oxide.

The grain shapes of the samples are polyhedral and equiaxed, in accordance with the identified crystallographic cells: C cell or Q cell with parameters close to those of C cell (since there is very little difference between a' ($a' = a\sqrt{2}$) and c parameters of Q cell). GSs vary depending on sintering type and conditions, and also on the GSs of the initial powders. When x value varies from 0.98 to 1.27, the drop in maximum GS from 40 to 25 μm could be due to the decrease in sintering temperature from 1280 °C to 1180 °C as well as to the decrease in quenching temperature from 900 °C to 800 °C. When x changes from 1.27 to 1.54, the maximum GS increases from 25 to 33 μm, despite the decrease in initial powder GS and this could be due to the increase of the quenching temperature from 800 °C to 1180 °C. For $x = 1.78$ the maximum GS is diminished compared to that of $x = 1.54$ and thus is reduced to 19 μm. This could be due to the decrease in GS of the initial powders, as well as to the change in cooling conditions (quenching for $x = 1.54$ and slow cooling to ambient temperature for $x = 1.78$).

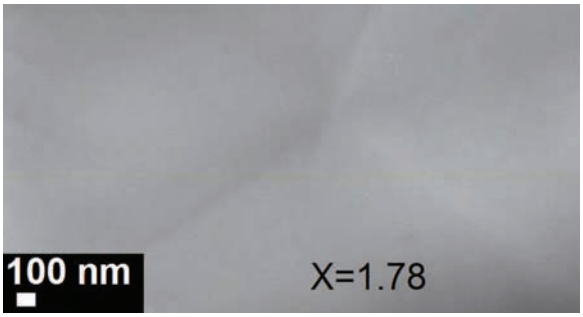

Fig. 10. Bright field TEM image of a single cubic phase $Mn_{3-x}Co_xO_4$ ceramic sample for $x = 1.78$ (conventionally sintered) showing a triple junction and the absence in each grain of twin defects.

For ceramic samples obtained by SPS (i.e., $x = 1.54$ and $x \geq 1.78$) the GSs are much smaller than those sintered by the conventional method and are relatively similar to those of the initial powders, which is predictable due to the fact that SPS sintering greatly reduces volume diffusion (i.e., grain coarsening) compared to conventional sintering.[60–63]

For $x < 1.78$, twins are well present in all ceramic samples, but they differ in their characteristics from sample to sample. The existence of twins in these samples could be due to the fact that the structural transition is ferroelastic, as it is in Mn_3O_4 hausmannite.[21] In fact, ferroelastic transition, which belongs to ferroic transitions, is able to produce structural domains with different orientation states under adapted conditions.[64–68] In this case, structural domains occur in materials to accommodate the constraints accompanying the phase transition since the latter leads, amongst others, to a reduction of crystallographic symmetry elements and a deformation of the crystallographic cell evaluated by the value of c/a' (a' (i.e., $a\sqrt{2}$) and c corresponds to Q cell parameters) with respect to the high-temperature phase. The twins arising in this case are called transformation twins. We can also note that the structure of the samples studied in this work, obey the fact that the point group symmetry of the low-temperature phase (4/mmm) is a subgroup of that of the high-temperature phase (m3m) and

thus the structural transition of these samples belongs to Aizu species m3mF4/mmm in his nomenclature of ferroelastic phase transitions.[67] The results obtained from electron microscopy revealed that the twins observed in these samples correspond to 1 1 2 twins (i.e., the twin interface plane is (1 1 2)). These results are in conformity with the theoretical predictions[65,66] about the ($h\,k\,l$) twin interface planes that may exist when a ferroelastic phase transition occurs from C phase with (m3m) point group symmetry to Q phase with (4/mmm) point group symmetry (h, k and l are the Miller indices). Considering changes in the characteristics of twins for $x < 1.78$, we can mention that the main factors which could have an effect on these variations are:

- increase in cell deformation c/a'.
- the fact that the chemical composition of the sample is near or far from the composition corresponding to the phase transition. For our samples this composition corresponds to $x = 1.78$ as indicated by the phase diagram of the Mn_3O_4–Co_3O_4 system reported in previous works.[48]
- the variation of GSs.

For $x = 1.66$, TEM observations indicate the existence, in this sample, of tweed domains shown by a modulated image contrast in two directions with widths on the order of a few nm. This result could be attributed to the fact that the chemical composition of this sample is close to that of the phase transition (i.e., $x = 1.78$) and thus could be noted as one of the features highlighting the ferroelastic character of the phase transition in $Mn_{3-x}Co_xO_4$. This is because many experimental and theoretical studies have shown the apparition of tweeds when approaching the phase transition in the case of ferroelastic transitions.[26,55,64,68–70] Among the various interpretations in this regard and taking into account that the sample used in this study has an homogeneous chemical composition (within the resolution of the analyses) and contains only one phase, we note that the observed tweeds could be related to the fact that, close to the phase transition, DW motion leads the microstructure to assume a stable arrangement corresponding to a minimum free energy value (including elastic energy) and which is consistent with strains induced by the phase transformation. Thus, this arrangement is established with the tweed microstructure and is compatible with the c/a' sample deformation which is of about 3.15% and is the lowest value compared to those of the others samples with $x < 1.78$.

When x decreases from 1.66 to 1.54, the chemical composition of the sample becomes a little bit far from that of the phase transition and the TEM observations reveal that the modulated microstructure is entirely replaced by twin domains corresponding to parallel L lamellae. As mentioned above, for the same chemical composition (i.e., $x = 1.54$), the decrease in lamella widths of the sample sintered by SPS compared to those of the sample obtained by conventional sintering could be due to the decrease in GSs induced by SPS sintering, in accordance with that has been reported in the literature.[54–57] For both samples (i.e., SPS and conventionally sintered samples), the value of the c/a' deformation is of about 4.6%, not excessively large in comparison to those of the other samples with lower values of x. However, when x decreases from 1.54 to 1.27, the increase in strain caused by the enhancement of the c/a' value could lead to enlargement of the lamellae as well as the formation inside them of new fine twin lamellae l, corresponding to internal twinning. In fact, as has been reported in the literature,[71] for a sample microstructure, there are potential sites for the formation of twins and when the deformation increases, twins are formed at these sites. Thus, the increase in deformation when going from 1.54 to 1.27, could generate an increase in the twin interface energy and then the activation of the sites that give rise to internal twins. The occurrence of these latters is promoted by the increase in the widths of the initial twin lamellae.

Then, a decrease in x from 1.27 to 0.98 is also accompanied by an increase in c/a' deformation, which could be contribute, on the one hand, to a large increase in width of the (L_{IT}) lamellae (more than twice the width of the (L_{IT}) lamellae for $x = 1.27$) and on the other hand, to the apparition of new fine internal twins (i.e., to the increase in internal twin density) and could ultimately lead to internal twin widths a little thinner than for $x = 1.27$. Also for $x = 0.98$ the L_{IT} lamellae are sometimes arranged in cyclic forms corresponding particularly to triangular shapes observed for the first time in manganites. In the literature, twins for which arrangement shapes are like three-pointed stars, not triangles, have been reported for ferroelastic phase transitions and have been attributed to the loss of the 3-fold axis of the high-temperature phase.[66]

Furthermore, it is well known that the activation energy of incoherent DW is much higher than that of coherent DW.[21,26,72] Thus, a significant increase in activation energy caused by the presence of incoherent DW could lead to a decrease in cation site exchange. In light of the fact that a large proportion of the material volume corresponds to DW, the incoherent ones which are present when $x < 1.54$ could contribute, in addition to other factors (related to cation distributions and which are mentioned in previous works),[42,46] to the fact that the variation in electrical resistivity of these ceramics shows a very large increase for $0.98 \leq x < 1.54$.

For $x \geq 1.78$, no defects were observed in these ceramic samples with C spinel structure (for $x = 1.78$, this result remains valid for both samples, i.e., SPS and conventionally sintered samples). This could be due to the absence of phase transition for these chemical compositions as it has been shown by the phase diagram of the Mn_3O_4–Co_3O_4 system.[48]

5. Conclusion

The microstructure of cobalt manganese oxide ceramics is presented, for the first time, in this paper. The studied samples correspond to single phase $Mn_{3-x}Co_xO_4$ ($0.98 \leq x \leq 2.93$) spinel ceramics and their microstructures were determined using TEM and EDX. They were obtained by conventional sintering or by SPS of powders (elaborated by thermal decomposition of coprecipitated oxalate precursors). Single Q phase and single C phase were obtained respectively for $x < 1.78$ and $x \geq 1.78$. Q phase occurs by the structural transition of C phase in agreement with the phase diagram of the Mn_3O_4–Co_3O_4 system.[48]

The structural transition of these samples belongs to Aizu species m3mF4/mmm in his nomenclature of ferroelastic phase transitions.[67] Samples with $x < 1.78$ show grains with high domain densities (i.e. twin densities) which could be due to the fact that the structural transition is ferroelastic. Coherent twin interface planes are parallel to (1 1 2) planes in the Q cell which is in accordance with theoretical predictions[65,66] for a ferroelastic phase transition occuring from C phase with (m3m) point group symmetry to Q phase with (4/mmm) point group symmetry.

The twins that are present in ceramic samples with $x < 1.78$, correspond to: tweeds, single lamellae, i.e., L (widths: 5–306 nm) arranged parallel to each other (and whose forms correspond to either right-angled twins or needle-shaped twins), large lamellae, i.e., L_{IT} (widths: 69–928 nm) internally twinned and sometimes arranged in cyclic forms corresponding to triangular shapes observed for the first time in manganites. Variations in the characteristics of twins were investigated in relation to: the variation of the cell deformation c/a', the fact that the chemical composition of the sample is near or far from the composition corresponding to the phase transition (i.e., $x = 1.78$) and the GS variations. The incoherent twin interfaces present for $x < 1.54$ could have an effect (in addition to other effects related to cation distributions and mentioned in previous works[42,46]) on the important increase in electrical resistivity for $x < 1.54$ because it is well-known that the activation energy of an incoherent twin interface is very much higher than that of coherent twin interface.

No defects were observed in ceramic samples corresponding to C phase (i.e., $x \geq 1.78$) which could be related to the absence of phase transition for these chemical compositions.

Acknowledgments

The authors would like to thank Mr. Laurent Weingarten (Service Commun de Microscopie Electronique TEMSCAN – Université Paul Sabatier – Toulouse) for his kind help in the preparation of samples for TEM observations.

References

1. Van Santen JH, Jonker GH. Electrical conductivity of ferromagnetic compounds of manganese with perovskite structure. *Physica* 1950;**16**(7–8):599–600.
2. Finch GI, Sinha APB, Sinha KP. Crystal distortion in ferrite-manganites. *Pro R Soc Lond A Math Phys Sci* 1957;**242**(1228):28–35.
3. Goodenough JB, Loeb AL. Theory of ionic ordering, crystal distortion, and magnetic exchange due to covalent forces in spinels. *Phys Rev* 1955;**98**(2):391–408.
4. Zener C. Interactions between the d shells in the transition metals. *Phys Rev* 1951;**81**:440–4.
5. Caffin JP, Rousset A, Carnet R, Lagrange A. Chemical preparation of NTC thermistors with low resistivity and high stability. In: Vencenzini P, editor. *High Tech Ceramics*. Amsterdam: Elsevier; 1987. p. 1743–51.
6. Guillemet-Fritsch S, Chanel C, Sarrias J, Bayonne S, Rousset A, Alcobe X, et al. Structure, thermal stability and electrical properties of zinc manganites. *Solid State Ionics* 2000;**128**(1–4):233–42.
7. Jabry E, Boissier G, Rousset A, Carnet R, Lagrange A. Preparation of semiconducting ceramics (NTC thermistors) by chemical method. *J Phys Colloques* 1986;**47**:C1 843–847.
8. Rousset A, Legros R, Lagrange A. Recent progress in the fabrication of ceramic negative temperature coefficient thermistors. *J Eur Ceram Soc* 1994;**13**(3):185–95.
9. Battault T, Legros R, Brieu M, Couderc JJ, Bernard L, Rousset A. Correlation between microstructure and ageing of iron manganite thermistors. *J Phys III (France)* 1997;**7**(5):979–92.
10. Metz R. Electrical properties of N.T.C. thermistors made of manganite ceramics of general spinel structure: $Mn_{3-x-x'}M_xN_{x'}O_4 (0 \leq x + x' \leq 1$; M and N being Ni, Co or Cu). Aging phenomenon study. *J Mater Sci* 2000;**35**:4705–11.
11. Sachse HB. *Semiconducting temperature sensors and their applications*. New York: Wiley; 1975.
12. Umadevi P, Nagendra CL. Preparation and characterisation of transition metal oxide micro-thermistors and their application to immersed thermistor bolometer infrared detectors. *Sens Actuators A Phys* 2002;**96**(2):114–24.
13. Kopia LP, Lee III RB. Thermistor bolometer scanning radiometer: applications and flight experience. *Opt Eng* 1992;**31**(1):156–65.
14. Sheftel IT. *Thermistors*. Moscow: Nauka; 1973.
15. Aleksić OS, Nikolić PM, Simić MN, Pejović VŽ, Vasiljević-Radović DG. Resistivity versus geometry relation in bulk-sintered and thick film MnCoFe-oxide thermistors. In: Stojanović BD, Skorokhod VV, Nikolić MV, editors. *Advanced science and technology of sintering*. New York: Kluwer Academic, Plenum Publishers; 1999. p. 425–30.
16. Aleksić OS, Savić SM, Luković MD, Radulović KT, Lukić LS. Segmented thermistors printed by NTC nanometric paste and applied in volume air-flow sensors. *Mater Sci Forum* 2006;**518**:247–52.
17. Edwards L, Murthy R. Versatile thermistors for wide-ranging applications. *Electrotechnology* 1987;**15**:89–91.
18. Metz R, Brieu M, Legros R, Rousset A. Intergranular phases in electroceramics. *J Phys Colloques* 1990;**51**:C1 1003–1008.
19. Brieu M, Couderc JJ, Rousset A, Legros R. TEM characterization of nickel and nickel–cobalt manganite ceramics. *J Eur Ceram Soc* 1993;**11**(2):171–7.
20. Rousset A, Lagrange A, Brieu M, Couderc JJ, Legros R. Influence de la microstructure sur la stabilité électrique des thermistances CTN. *J Phys III (France)* 1993;**3**:833–45.
21. Couderc JJ, Fritsch S, Brieu M, Vanderschaeve G, Fagot M, Rousset A. A transmission electron microscopy study of lattice defects in Mn_3O_4 hausmannite. *Phil Mag B* 1974;**70**(5):1077–94.
22. Couderc JJ, Fritsch S, Brieu M, Vanderschaeve G. A transmission electron microscopy study of accomodation twins in Ba–Ni–Mn oxides. *Phil Mag A* 1996;**74**(6):1351–65.
23. Fritsch S, Sarrias J, Brieu M, Couderc JJ, Baudour JL, Snoeck E, et al. Correlation between the structure, the microstructure and the electrical properties of nickel manganite negative temperature coefficient (NTC) thermistors. *Solid State Ionics* 1998;**109**:229–37.
24. Martin De Vidales JL, Garcia-Chain P, Rojas RM, Vila E, Garcia-Martinez O. Preparation and characterization of spinel-type Mn–Ni–Co–O negative temperature coefficient ceramic thermistors. *J Mater Sci* 1998;**33**:1491–6.
25. Chanel C. *Optimisation des caractéristiques structurales, microstructurales et électriques des manganites de nickel, de zinc et de nickel-zinc en vue de l'application aux thermistances à coefficient de température négatif (CTN)*. Thèse de Doctorat de l'Université de Toulouse; 1998.
26. Metzmacher C, Groen WA, Reaney IM. Microstructure and electrical properties of Mn–Ni–In spinels. *Phys Stat Sol* 2000;**181**:369–86.
27. Park K. Microstructure and electrical properties of $Ni_{1.0}Mn_{2-x}Zr_xO_4$ $(0 \leq x \leq 1.0)$ negative temperature coefficient thermistors. *Mater Sci Eng B* 2003;**104**:9–14.
28. Park K, Han IH. Effect of Al_2O_3 addition on the microstructure and electrical properties of $Mn_{0.37}Ni_{0.3}Co_{0.33-x}Al_xO_4$ $(0 \leq x \leq 0.03)$ NTC thermistors. *Mater Sci Eng B* 2005;**119**:55–60.
29. Park K, Lee JK, Kim SJ, Seo WS, Cho WS, Lee CW, et al. The effect of Zn on the microstructure and electrical properties of $Mn_{1.17-x}Co_{0.93}Co_{0.9}Zn_xO_4$ $(0 \leq x \leq 0.075)$ NTC thermistors. *J Alloys Compd* 2009;**467**:310–6.
30. Bodak O, Akselrud P, Demchenko P, Kotur B, Mrooz O, Hadzaman I, et al. Microstructure, crystal structure and electrical properties of $Cu_{0.1}Ni_{0.8}Co_{0.2}Mn_{1.9}O_4$ ceramics obtained at different sintering conditions. *J Alloys Compd* 2002;**347**:14–23.

31. Varghese JM, Seema A, Dayas KR. Ni–Mn–Fe–Cr–O negative temperature coefficient thermistor compositions: correlation between processing conditions and electrical characteristics. *J Electroceram* 2009;**22**(4):436–41.
32. Park K. Fabrication and electrical properties of Mn–Ni–Co–Cu–Si oxides negative temperature coefficient thermistors. *J Am Ceram Soc* 2005;**88**(4):862–6.
33. Varghese JM, Seema A, Dayas KR. Microstructural electrical and reliability aspects of chromium doped Ni–Mn–Fe–O NTC thermistor materials. *Mater Sci Eng B* 2008;**149**:47–52.
34. Borges FMM, Melo DMA, Câmara MSA, Martinelli AE, Soares JM, de Araújo JH, et al. Magnetic behavior of nanocrystalline $MnCo_2O_4$ spinels. *J Magn Magn Mater* 2006;**302**:273–7.
35. Vasil'ev GP, Pakhomov LA, Ryabova LA. Structural and electrical properties of d.c. sputtered $MnCo_2O_4$ films. *Thin Solid Films* 1980;**66**:119–24.
36. Rios E, Poillerat G, Koenig JF, Gautier JL, Chartier P. Preparation and characterization of thin Co_3O_4 and $MnCo_2O_4$ films prepared on glass/SnO_2:F by spray pyrolysis at 150 °C for the oxygen electrode. *Thin Solid Films* 1995;**264**:18–24.
37. Martin de Vidales JL, Vila E, Rojas RM, Garcia-Martinez O. Thermal behavior in air and reactivity in acid medium of cobalt manganese spinels $Mn_xCo_{3-x}O_4$ $(1 \leq x \leq 3)$ synthesized at low temperature. *Chem Mater* 1995;**7**(9):1716–21.
38. Kolomiets BT, Sheftel J, Kurlina E. Electrical properties of some compound oxide semiconductors. *Sov Phys Tech Phys* 1957;**2**:40–58.
39. Wickham DG, Croft WJ. Crystallographic and magnetic properties of several spinels containing trivalent ja-1044 manganese. *J Phys Chem Solids* 1958;**7**:351–60.
40. Jabry EH, Rousset A, Lagrange A. Preparation and characterization of manganese and cobalt based semiconducting ceramics. *Phase Transitions* 1988;**13**(1–4):63–71.
41. Buhl R. Manganites spinelles purs d'éléments de transition préparations et structures cristallographiques. *J Phys Chem Solids A* 1969;**30**(4):805–12.
42. Bordeneuve H, Guillemet-Fritsch S, Rousset A, Shuurman S, Poulain V. Structure and electrical properties of single-phase cobalt manganese oxide spinels $Mn_{3-x}Co_xO_4$ sintered classically and by spark plasma sintering (SPS). *J Solid State Chem* 2009;**182**(2):396–401.
43. Bordeneuve H, Tenailleau C, Guillemet-Fritsch S, Smith R, Suard E, Rousset A. Structural variations and cation distributions in $Mn_{3-x}Co_xO_4$ $(0 \leq x \leq 3)$ dense ceramics using neutron diffraction data. *Solid State Sci* 2010;**12**(3):379–86.
44. Bordeneuve H, Rousset A, Tenailleau C, Guillemet-Fritsch S. Cation distribution in manganese cobaltite spinels $Co_{3-x}Mn_xO_4$ $(0 \leq x \leq 1)$ determined by thermal analysis. *J Thermal Anal Calorim* 2010;**101**(1):137–42.
45. Guillemet-Fritsch S, Tenailleau C, Bordeneuve H, Rousset A. Magnetic properties of cobalt and manganese oxide spinel ceramics. *Adv Sci Tech* 2010;**67**:143–8.
46. Rousset A, Tenailleau C, Dufour P, Bordeneuve H, Pasquet I, Guillemet-Fritsch S, et al. Electrical properties of $Mn_{3-x}Co_xO_4$ $(0 \leq x \leq 3)$ ceramics: an interesting system for negative temperature coefficient thermistors. *Int J Appl Ceram Technol* 2013;**10**(1):175–85.
47. Bordeneuve H. *Etude du système $Mn_{3-x}Co_xO_4$ $(0 \leq x \leq 3)$ sous forme de poudres et de céramiques. Structure, microstructure, propriétés magnétiques et électriques. Applications aux thermistances à Coefficient de Température Négatif (C.T.N.)*. Thèse de Doctorat de l'Université de Toulouse; 2009.
48. Aukrust E, Muan A. Thermodynamic properties of solid solutions with spinel-type structure. I: The system Co_3O_4–Mn_3O_4. *Trans Met Soc AIME* 1964;**230**:378–82.
49. Abramoff MD, Magelhaes PJ, Ram SJ. Image processing with ImageJ. *Biophotonics Int* 2004;**11**(7):36–42.
50. Salje EKH, Ishibashi Y. Mesoscopic structures in ferroelastic crystals: needle twins and right-angled domains. *J Phys Condens Matter* 1996;**8**:8477–95.
51. Salje EKH, Buckley A, Van Tendeloo G, Ishibashi Y, Nord JrG.L. Needle twins and right-angled twins in minerals: comparison between experiment and theory. *Am Mineral* 1998;**83**:811–22.
52. Buckley A, Rivera JP, Salje EKH. Twin structures in tetragonal $SrTiO_3$: the ferroelastic phase transition and the formation of needle domains. *J Appl Phys* 1999;**86**(3):1653–6.
53. Orlovskaya N, Browning N, Nicholls A. Ferroelasticity in mixed conducting $LaCoO_3$ based perovskites: a ferroelastic phase transition. *Acta Mater* 2003;**51**:5063–71.
54. Zhu L, Ruan H, Li X, Dao M, Gao H, Lu J. Modeling grain size dependent optimal twin spacing for achieving ultimate high strength and related high ductility in nanotwinned metals. *Acta Mater* 2011;**59**(14):5544–57.
55. Salje EKH. *Phase transitions in ferroelastic and coelastic crystals*. Cambridge University Press; 1990.
56. Cao W, Randall CA. Grain size and domain size relations in bulk ceramic ferroelectric materials. *J Phys Chem Solids* 1996;**57**(10):1499–505.
57. El-Danaf E, Kalidindi SR, Doherty RD. Influence of grain size and stacking-fault energy on deformation twinning in fcc metals. *Metall Mater Trans A* 1999;**30**:1223–33.
58. Robbrecht GG, Henriet-Iserentant CM. On the lattice parameters and the tetragonal distortion of the copper and cadmium manganite systems. *Phys Status Solidi (b)* 1970;**41**(1):K43–6.
59. Gautier JL, Meza E, Silva E, Lamas C, Silva C. Effect of the $ZnNi_yMn_{2-y}O_4$ $(0 \leq y \leq 1)$ spinel composition on electrochemical lithium insertion. *J Solid State Electrochem* 1997;**1**(2):126–33.
60. Hungría T, Galy J, Castro A. Spark plasma sintering as a useful technique to the nanostructuration of piezo-ferroelectric materials. *Adv Eng Mater* 2009;**11**(8):615–31.
61. Chaim R, Shen Z. Grain size control by pressure application regime during spark plasma sintering of Nd-YAG nanopowders. *J Mater Sci* 2008;**43**:5023–7.
62. Rajeswari K, Hareesh US, Subasri R, Chakravarty Dibyendu, Johnson R. Comparative evaluation of spark plasma (SPS), microwave (MWS), two stage sintering (TSS) and conventional sintering (CRH) on the densification and microstructural evolution of fully stabilized zirconia ceramics. *Sci Sinter* 2010;**42**:259–67.
63. Lu K. *Nanoparticulate materials: synthesis, characterization and processing*. Wiley; 2013.
64. Salje EKH, Hayward SA, Lee WT. Ferroelastic phase transitions: structure and microstructure. *Acta Crystallogr A* 2005;**61**(1):3–18.
65. Sapriel J. Domain-wall orientations in ferroelastics. *Phys Rev B* 1975;**12**:5128–40.
66. Boulesteix C. A survey of domains and domain walls generated by crystallographic phase transitions causing a change of the lattice. *Phys Status Solidi (a)* 1984;**86**(1):11–42.
67. Aizu K. Possible species of ferromagnetic, ferroelectric and ferroelastic crystals. *Phys Rev B* 1970;**2**:754–72.
68. Tagantsev AK, Cross TL. *Domains in ferroic crystals and thin films*. Springer; 2010.
69. Meng X, Baba-Kishi KZ, Pang GKH, Chan HL, Choy CL, Luo HS. Tweed domains in ferroelectrics with compositions at the morphotropic phase boundary. *Phil Mag Lett* 2004;**84**(3):191–7.
70. Tribaudino M, Benna P, Bruno E. I1–I2/c phase transition in alkaline-earth feldspars: evidence from TEM observations of Sr-rich feldspars along the $CaAl_2Si_2O_8$–$SrA1_2Si_2O_8$ join. *Am Mineral* 1995;**80**:907–15.
71. Putnis A. *Introduction to mineral sciences*. Cambridge University Press; 1992.
72. Priester L. *Les joints de grains de la théorie à l'ingénierie*. EDP Sciences; 2006.